Dynamic phase transition in the kinetic spin-3/2 Blume-Capel model under a time-dependent oscillating external field

Mustafa Keskin, Osman Canko, and Bayram Deviren
Department of Physics, Erciyes University, 38039 Kayseri, Turkey
(Received 6 March 2006; published 17 July 2006)

We present a study, within a mean-field approach, of the stationary states of the kinetic spin-3/2 Blume-Capel model in the presence of a time-dependent oscillating external magnetic field. We use the Glauber-type stochastic dynamics to describe the time evolution of the system. We have found that the behavior of the system strongly depends on the crystal-field interaction. We can identify two types of solutions: a symmetric one where the magnetization (m) of the system oscillates in time around zero, which corresponds to a paramagnetic phase (P), and an antisymmetric one where m oscillates in time around a finite value different from zero, namely $\pm 3/2$ and $\pm 1/2$ that corresponds to the ferromagnetic-3/2 ($F_{3/2}$) and the ferromagnetic-1/2 ($F_{1/2}$) phases, respectively. There are coexistence regions of the phase space where the $F_{3/2}$, $F_{1/2}$ ($F_{3/2}+F_{1/2}$), $F_{3/2}$, P ($F_{3/2}+P$), $F_{1/2}$, P ($F_{1/2}+P$), and $F_{3/2}$, $F_{1/2}$, P ($F_{3/2}+F_{1/2}+P$) phases coexist, hence the system exhibits seven different phases. We obtain the dynamic phase transition points and find six fundamental phase diagrams which exhibit one or three dynamic tricritical points. We have also calculated the Liapunov exponent to verify the stability of the solutions and the dynamic phase transition points.

DOI: 10.1103/PhysRevE.74.011110 PACS number(s): 05.50.+q, 05.70.Fh, 64.60.Ht, 75.10.Hk

I. INTRODUCTION

The Ising models have been one of the most extensively studied systems in statistical and condensed-matter physics and have also been used as elementary models for a variety of phenomena. This is so not only because of the relative simplicity with which approximate calculations for these models can be carried out and tested, but also because versions and extensions of models can be applied to a wide class of real systems. Although the majority of studies have focused on spin-1/2 and spin-1 Ising models, higher spin systems are not without interest. One of the important higher spin systems is a spin-3/2 Ising model which has been paid much attention to for many years. The spin-3/2 Ising model Hamiltonian with arbitrary bilinear (J) and biquadratic (K) nearest-neighbor interactions, has been introduced earlier [1] to give a qualitative description of phase transitions observed in the compound $DyVO_4$ within the mean-field approximation (MFA). Later on, the spin-3/2 Ising model contains a crystal-field interaction or single-ion anisotropy (D) in addition to J and K exchange interactions, also known as the spin-3/2 Blume-Emery-Griffiths (BEG) model, was used in a study of tricritical properties of a ternary fluid mixture and compared with the results of the experimental observations on the systems of ethanol-water-carbon dioxide [2]. Since then, there have been large theoretical efforts devoted to the study of critical, magnetic, and thermodynamic properties and as well as phase diagrams and multicritical behavior of the spin-3/2 Ising systems by using the well-known methods in equilibrium statistical physics [3]. Recently, random spin-3/2 antiferromagnetic Heisenberg chains [4] and the random quantum antiferromagnetic spin-3/2 chain [5] have been studied using the renormalization group (RG) calculations.

On the other hand, a spin-3/2 Ising system containing crystal-field interaction (D) in addition to the bilinear exchanged interaction (J) is often called the spin-3/2 Blume-Capel (BC) model. The ferromagnetic spin-3/2 BC model has been studied within the effective field theory (EFT) [6–8], the mean field approximation (MFA) [9], the two-spin cluster approximation in the cluster expansion method [10], conventional finite-size scaling, conformal invariance, and Monte Carlo (MC) simulations [11], the pair approximation for the free energy, MC simulations [12], a thermodynamically self-consistent theory based on an Ornstein-Zernike approximation [13], and extensive MC simulations [14]. The exact solution of the ferromagnetic spin-3/2 BC model was presented on the Bethe lattice by means of the exact recursion relations [15]. Moreover, an early attempt to study the antiferromagnetic spin-3/2 BC model was made by Bakchich *et al.* [16]. They studied the multicritical behavior of the model with an antiferromagnetic bilinear interaction ($J<0$), with a crystal field (D) and under an external magnetic field (H) by using the MFA. Bekhechi and Benyoussef [17] investigated the multicritical behavior of the antiferromagnetic spin-3/2 BC model by using the transfer-matrix finite-size-scaling (TMFSS) calculations and MC simulations. Ekiz [18] investigated the antiferromagnetic spin-3/2 BC model on the Bethe lattice in an external magnetic field by using the recursion method. Recently, Keskin *et al.* [19] studied the antiferromagnetic spin-3/2 BC model in the presence of an external magnetic field within the cluster variation method.

While much work has been done on the equilibrium properties of the spin-3/2 BC model, to our knowledge, there has been only one investigation about the dynamical aspects of the model which were done by Grandi and Figueiredo [20]. They employed the MC simulations and short-time dynamic scaling to determine the static and dynamic critical exponents for the two-dimensional spin-3/2 BC model and discussed critical exponents, extensively. We should also mention that the dynamic behavior of the spin-3/2 Ising model Hamiltonian with bilinear (J) and biquadratic (K) nearest-neighbor pair interactions, also known as the isotropic spin-3/2 Blume-Emery-Grifftihs (BEG) model, was studied by

the path probability method (PMM) with point distribution, especially the relaxation of the order parameters which were investigated in Ref. [21]. The dynamic behavior of the model was also shown in a three-dimensional phase space. Moreover, the dynamics of the isotropic spin-3/2 BEG model was also studied near the second-order phase transition temperature by means of Onsager's theory of irreversible thermodynamics, in particular three relaxation times were calculated and examined for the temperatures near the second-order phase transition temperatures [22].

The purpose of this paper is to study, within a mean-field approach, the kinetic spin-3/2 Blume-Capel model in the presence of a time-dependent oscillating external magnetic field by the Glauber stochastic dynamics. More precisely, we obtain the nonequilibrium or dynamic phase transition (DPT) points and present phase diagrams in the reduced magnetic field amplitude and reduced temperature plane. We also calculate the Liapunov exponent to verify the stability of the solutions and the DPT points.

We should also mention that the DPT was first found in a study within a mean-field approach, the stationary states of the kinetic spin-1/2 Ising model under a time-dependent oscillating field [23,24], by using the Glauber-type stochastic dynamics [25], and it was followed by a Monte Carlo simulation, which allows the microscopic fluctuations, research of kinetic spin-1/2 Ising models [26–28], as well as further mean-field studies [29]. Moreover, Tutu and Fujiwara [30] developed the systematic method for the phase diagrams in DPTs, and constructed the general theory of DPTs near the transition point based on the mean-field description, such as Landau's general treatment of the equilibrium phase transitions. The DPT has also been found in a one-dimensional kinetic spin-1/2 Ising model with boundaries [31]. Reviews of earlier research on the DPT and related phenomena are found in Ref. [28]. We should also mention that recent research on the DPT is widely extended to more complex systems such as vector-type order parameter systems, e.g., the Heisenberg-spin systems [32], *XY* model [33], a Ziff-Gulari-Barshad model for CO oxidation with CO desorption to periodic variation of the CO pressure [34], a high-spin Ising models such as the kinetic spin-1 BC model [35], and a mixed-spin Ising model, e.g., the kinetics of a mixed spin-1/2 and spin-1 Ising model [36].

Finally, it is worthwhile to mention that the study of phase transitions and critical phenomena in nonequilibrium systems is a subject of great interest in a broad range of fields such as chemical reactions, fluid turbulence, chaos, biological populations, growth-deposition processes, and even economics [37]. These systems not only exhibit rich and complex critical phenomena associated with out-of-equilibrium statistical physics, but they can also play an important role in explaining a wide range of experimental results. Especially, the study of surface reaction systems [38] and thin ferromagnetic films [39] has received a great deal of attention. Moreover, experimental evidences for the DPT have been found in highly anisotropic (Ising-like) and ultrathin Co/Cu(001) ferromagnetic films [40] and in ferroic systems (ferromagnets, ferroelectrics and ferroelastics) with pinned domain walls [41].

The outline of the remaining part of this paper is organized as follows. In Sec. II, the spin-3/2 BC model is briefly described and the derivation of the dynamic equation of motion is given. In Sec. III, the DPT points are calculated and the phase diagrams are presented. The paper ends with a summary of the work in Sec. IV.

II. THE MODEL AND DERIVATION OF MEAN-FIELD DYNAMICAL EQUATION

The spin-3/2 BC model in the presence of a time-dependent oscillating external magnetic field is described by the following Hamiltonian:

$$H = -J\sum_{\langle ij\rangle} S_i S_j - D\sum_i S_i^2 - H\sum_i S_i, \tag{1}$$

where the S_i located at the site i on a discrete lattice can take the values $\pm 3/2$ and $\pm 1/2$ at each site i of a lattice and $\langle ij\rangle$ indicates the summation over all pairs of nearest-neighbor sites. The first term describes the ferromagnetic coupling ($J>0$) between the spins at sites i and j. This interaction is restricted to z-nearest-neighbor pairs of spins. The second term describes the crystal field-interaction and the last term, H, represents a time-dependent external oscillating magnetic field. H is given by

$$H(t) = H_0 \cos(wt), \tag{2}$$

where H_0 and $w=2\pi\nu$ are the amplitude and the angular frequency of the oscillating field, respectively. The system is in contact with an isothermal heat bath at absolute temperature.

Now, we will apply the Glauber-type stochastic dynamics to obtain the dynamic equation of motion. Hence, the system evolves according to a Glauber-type stochastic process at a rate of $1/\tau$ transitions per unit time. We define $P(S_1,S_2,\ldots,S_N;t)$ as the probability that the system has the S spin configuration, $S_1,S_2,\ldots,S_N$, at time t. The time dependence of this probability function is assumed to be governed by the master equation which describes the interaction between the spins and heat bath and can be written as follows:

$$\begin{aligned}\frac{d}{dt}P(S_1,S_2,\ldots,S_N;t) = &-\sum_i \left(\sum_{S_i\neq S_i'} W_i(S_i\to S_i')\right)\\ &\times P(S_1,S_2,\ldots,S_i,\ldots,S_N;t)\\ &+\sum_i \left(\sum_{S_i\neq S_i'} W_i(S_i'\to S_i)\right.\\ &\left.\times P(S_1,S_2,\ldots,S_i',\ldots,S_N;t)\right),\end{aligned} \tag{3}$$

where $W_i(S_i\to S_i')$, the probability per unit time that the ith spin changes from the value S_i to S_i', and in this sense the Glauber model is stochastic. Since the system is in contact with a heat bath at absolute temperature T, each spin can change from the value S_i to S_i' with the probability per unit time;

$$W_i(S_i \to S_i') = \frac{1}{\tau} \frac{\exp[-\beta \Delta E(S_i \to S_i')]}{\sum_{S_i'} \exp[-\beta \Delta E(S_i \to S_i')]}, \tag{4}$$

where $\beta = 1/k_B T$, k_B is the Boltzmann factor, $\Sigma_{S_i'}$ is the sum over the four possible values of S_i', $\pm 3/2$, $\pm 1/2$, and ΔE is the change in the energy of the system when the S_i spin changes, which can be found by working Eq. (1). Using the detailed balance condition [35,36], we get

$$W_i\left(\frac{3}{2} \to \frac{3}{2}\right) = W_i\left(\frac{1}{2} \to \frac{3}{2}\right) = W_i\left(-\frac{1}{2} \to \frac{3}{2}\right) = W_i\left(-\frac{3}{2} \to \frac{3}{2}\right)$$
$$= \frac{1}{2\tau} \frac{\exp(\beta D)\exp(3\beta x/2)}{\exp(\beta D)\cosh(-3\beta x/2) + \exp(-\beta D)\cosh(-\beta x/2)}, \tag{5a}$$

$$W_i\left(\frac{3}{2} \to \frac{1}{2}\right) = W_i\left(\frac{1}{2} \to \frac{1}{2}\right) = W_i\left(-\frac{1}{2} \to \frac{1}{2}\right) = W_i\left(-\frac{3}{2} \to \frac{1}{2}\right)$$
$$= \frac{1}{2\tau} \frac{\exp(-\beta D)\exp(\beta x/2)}{\exp(\beta D)\cosh(-3\beta x/2) + \exp(-\beta D)\cosh(-\beta x/2)}, \tag{5b}$$

$$W_i\left(\frac{3}{2} \to -\frac{1}{2}\right) = W_i\left(\frac{1}{2} \to -\frac{1}{2}\right) = W_i\left(-\frac{1}{2} \to -\frac{1}{2}\right) = W_i\left(-\frac{3}{2} \to -\frac{1}{2}\right)$$
$$= \frac{1}{2\tau} \frac{\exp(-\beta D)\exp(-\beta x/2)}{\exp(\beta D)\cosh(-3\beta x/2) + \exp(-\beta D)\cosh(-\beta x/2)}, \tag{5c}$$

$$W_i\left(\frac{3}{2} \to -\frac{3}{2}\right) = W_i\left(\frac{1}{2} \to -\frac{3}{2}\right) = W_i\left(-\frac{1}{2} \to -\frac{3}{2}\right) = W_i\left(-\frac{3}{2} \to -\frac{3}{2}\right)$$
$$= \frac{1}{2\tau} \frac{\exp(\beta D)\exp(-3\beta x/2)}{\exp(\beta D)\cosh(-3\beta x/2) + \exp(-\beta D)\cosh(-\beta x/2)}, \tag{5d}$$

where $x = H + J\Sigma_{\langle j \rangle} S_j$. Notice that, since $W_i(S_i \to S_i')$ does not depend on the value S_i, we can write $W_i(S_i \to S_i') = W_i(S_i')$, then the master equation becomes

$$\frac{d}{dt} P(S_1, S_2, \ldots, S_N; t) = -\sum_i \left(\sum_{S_i' \neq S_i} W_i(S_i') \right) P(S_1, S_2, \ldots, S_i, \ldots, S_N; t) + \sum_i W_i(S_i) \left(\sum_{S_i' \neq S_i} P(S_1, S_2, \ldots, S_i', \ldots, S_N; t) \right). \tag{6}$$

Since the sum of probabilities is normalized to one, by multiplying both sides of Eq. (6) by S_k and taking the average, we obtain

$$\tau \frac{d}{dt} \langle S_k \rangle = -\langle S_k \rangle + \left\langle \frac{3\exp(\beta D)\sinh\left(3\beta\left(J\sum_{\langle j \rangle} S_j + H\right)/2\right) + \exp(-\beta D)\sinh\left(\beta\left(J\sum_{\langle j \rangle} S_j + H\right)/2\right)}{2\exp(\beta D)\cosh\left(-3\beta\left(J\sum_{\langle j \rangle} S_j + H\right)/2\right) + 2\exp(-\beta D)\cosh\left(-\beta\left(J\sum_{\langle j \rangle} S_j + H\right)/2\right)} \right\rangle, \tag{7}$$

or, in terms of a mean-field approach,

$$\tau \frac{d}{dt} \langle S \rangle = -\langle S \rangle + \frac{3\exp(\beta D)\sinh[3\beta(Jz\langle S \rangle + H_0 \cos(wt))/2] + \exp(-\beta D)\sinh[\beta(Jz\langle S \rangle + H_0 \cos(wt))/2]}{2\exp(\beta D)\cosh[-3\beta(Jz\langle S \rangle + H_0 \cos(wt))/2] + 2\exp(-\beta D)\cosh[-\beta(Jz\langle S \rangle + H_0 \cos(wt))/2]}, \tag{8}$$

where z is the coordination number. The system evolves according to the differential equation given by Eq. (8), that can be written in the form

$$\Omega \frac{d}{d\xi} m = -m + \frac{3\exp(d/T)\sinh[3(m + h\cos\xi)/2T] + \exp(-d/T)\sinh[(m + h\cos\xi)/2T]}{2\exp(d/T)\cosh[-3(m + h\cos\xi)/2T] + 2\exp(-d/T)\cosh[-(m + h\cos\xi)/2T]}, \tag{9}$$

where $m \equiv \langle S \rangle$, $\xi = wt$, $T = (\beta z J)^{-1}$, $d = D/zJ$, $h = H_0/zJ$, and $\Omega = \tau w$. Hence, the mean-field dynamical equation for the magnetization is obtained. We fixed $z=4$ and $\Omega = 2\pi$. The solution and a discussion of this equation are given in the next section.

III. DYNAMIC PHASE TRANSITION POINTS AND PHASE DIAGRAMS

In this section, we shall find the dynamic phase transition (DPT) points and present the phase diagrams. For these purposes, first we have to study the stationary solutions of the dynamic equation, given in Eq. (9), when the parameters T, d, and h are varied. The stationary solution of Eq. (9) will be a periodic function of ξ with period 2π; that is, $m(\xi + 2\pi) = m(\xi)$. Moreover, it can be one of two types according to whether it has or does not have the property

$$m(\xi + \pi) = -m(\xi). \tag{10}$$

A solution that satisfies Eq. (10) is called a symmetric solution which corresponds to a paramagnetic (P) solution. In this solution, the magnetization $m(\xi)$ oscillates around the zero value and is delayed with respect to the external field. The second type of solution which does not satisfy Eq. (10) is called a nonsymmetric solution that corresponds to a ferromagnetic (F) solution. In this case the magnetization does not follow the external magnetic field any more, but instead of oscillating around a zero value; it oscillates around a nonzero value, namely either $\pm 3/2$ or $\pm 1/2$. Hence, if it oscillates around $\pm 3/2$, this nonsymmetric solution corresponds to the ferromagnetic $\pm 3/2$ ($F_{3/2}$) phase and if it oscillates around $\pm 1/2$, this corresponds to the ferromagnetic $\pm 1/2$ ($F_{1/2}$) phase. These facts are seen explicitly by solving Eq. (9) numerically. Equation (9) is solved by using the numerical method of the Adams-Moulton predictor corrector method for a given set of parameters and initial values and presented in Fig. 1. From Fig. 1, one can see seven different solutions, namely the P, $F_{3/2}$, $F_{1/2}$, and four coexistence solutions, namely the $F_{1/2}+P$ in which $F_{1/2}$, P solutions coexist; the $F_{3/2}+P$ in which $F_{3/2}$, P solutions coexist; the $F_{3/2}+F_{1/2}$ in which $F_{3/2}$, $F_{1/2}$ solutions coexist and the $F_{3/2}+F_{1/2}+P$ in which $F_{3/2}$, $F_{1/2}$, P solutions coexist, exist in the system. In Fig. 1(a) only the symmetric solution is always obtained, hence we have a paramagnetic (P) solution, but in Figs. 1(b) and 1(c) only the nonsymmetric solutions are found so therefore we have a ferromagnetic (F) solutions in which Fig. 1(b) corresponds to the $F_{1/2}$ phase and Fig. 1(c) to the $F_{3/2}$ phase. These solutions do not depend on the initial values. On the other hand, in Fig. 1(d) both the $F_{1/2}$ and P phases always exist in the system, hence we have the coexistence solution ($F_{1/2}+P$). In this case the solutions depend on the initial values, seen in Fig. 1(d) explicitly. Figures 1(e)–1(g) are similar to the Fig. 1(d), except $F_{3/2}$, P phases exist in Fig. 1(e); $F_{3/2}$, $F_{1/2}$ phases occur in Fig. 1(f) and $F_{3/2}$, $F_{1/2}$, P phases exist in Fig. 1(g). Therefore, we have four different coexistence solutions and these solutions depend on the initial values. We should also mention that for large values of h and T, the P phase always occurs in the system.

Thus, Fig. 1 displays seven different phases, namely the P, $F_{1/2}$, $F_{3/2}$, $F_{1/2}+P$, $F_{3/2}+P$, $F_{3/2}+F_{1/2}$, and $F_{3/2}+F_{1/2}+P$ phases, exist in the system. In order to obtain the dynamic phase boundaries among these phases, we have to calculate DPT points and then we can present phase diagrams of the system. DPT points will be obtained by investigating the behavior of the average magnetization in a period as a function of the reduced temperature. These investigations will be also checked and verified by calculating the Liapunov exponent.

The average magnetization (M) in a period, which is also called the dynamic magnetization, is given as

$$M = \frac{1}{2\pi} \int_0^{2\pi} m(\xi) d\xi. \tag{11}$$

The behavior of M as a function of the reduced temperature for several values of h and d are obtained by combining the numerical methods of Adams-Moulton predictor corrector with the Romberg integration and the results are plotted in Fig. 2 together. In this figure, the thick and thin arrows represent to the second-order phase transition (or the critical) temperatures, T_C (thick arrow) and $T_{C'}$ (thin arrow). T_C is the second-order phase transition temperature from the $F_{3/2}$ phase to the P phase and $T_{C'}$ from the $F_{1/2}$ phase to the P phase. Moreover, T_t represents the first-order phase transition temperature. Figure 2(a) shows the behavior of M as a function of the reduced temperature for the thick solid line; $d=-0.25$, $h=0.50$, and the thin solid line; $d=-0.5$, $h=1.25$. The system exhibits a second-order phase transition and the transition is from the $F_{3/2}$ phase to the P phase, for the thick solid line and from the $F_{1/2}$ phase to the P phase for the thin solid line in Fig. 2(a). Figures 2(b) and 2(c) illustrate the thermal variations of M for $d=-0.5$, $h=0.25$ for two different initial values; i.e., the initial value of M is taken 3/2 for Fig. 2(b) and 1/2 or zero for Fig. 2(c). In Fig. 2(b), the system undergoes two successive phase transitions: First, the phase transition is a first-order and the transition is from the $F_{3/2}$ phase to the $F_{1/2}$ phase, and the second one is a second-order phase transition from the $F_{1/2}$ phase to the P phase. This means that the coexistence region, i.e., the $F_{3/2}+F_{1/2}$ phase, exists in the system and this fact is seen in the phase diagram of Fig. 4(d) explicitly [compare in Figs. 2(b) and 2(c) with Fig. 4(d)]. Figures 2(d) and 2(e) illustrate the thermal variations of M for $d=-0.475$, $h=0.125$ for two different initial values; i.e., the initial value of M is taken 3/2 for Fig. 2(d) and 1/2 or zero for Fig. 2(e). These figures are similar to the Figs. 2(b) and 2(c), except the first-order phase transition is from the $F_{1/2}$ phase to the $F_{3/2}$ phase and the second-order phase transition from the $F_{3/2}$ phase to the P phase. Therefore, the $F_{3/2}+F_{1/2}$ phase occurs in the system [compare in Figs. 2(d) and 2(e) with Fig. 4(c)]. Figures 2(f) and 2(g) present the thermal variations of M for $d=0.25$, $h=1.025$ for two different initial values; i.e., the initial value of M is taken 3/2 or 1/2 for Fig. 2(f) and zero for Fig. 2(g). In Fig. 2(f), the system undergoes a second-order phase transition from the $F_{3/2}$ phase to the P phase. In Fig. 2(g), the system undergoes two successive phase transitions: First, the phase transition is a first-order from the P phase to the $F_{3/2}$

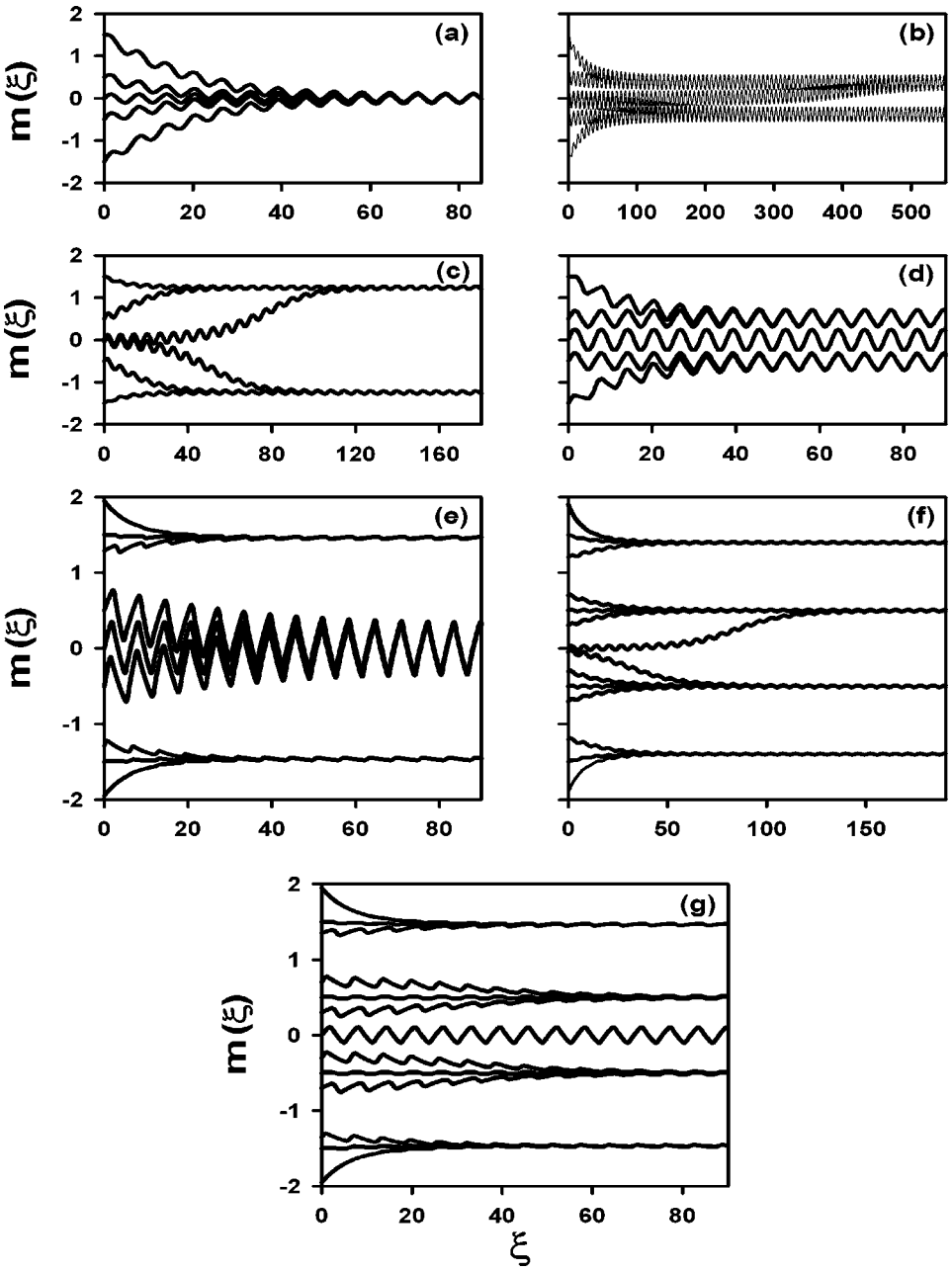

FIG. 1. Time variations of the magnetization (m): (a) Exhibiting a paramagnetic phase (P), $d=-0.75$, $h=1.0$, and $T=0.25$. (b) Exhibiting a ferromagnetic-1/2 ($F_{1/2}$) phase, $d=-0.5$, $h=1.125$, and $T=0.1875$. (c) Exhibiting a ferromagnetic-3/2 ($F_{3/2}$) phase, $d=-0.25$, $h=0.5$, and $T=0.5$. (d) Exhibiting a coexistence region ($F_{1/2}+P$), $d=-0.475$, $h=1.375$, and $T=0.025$. (e) Exhibiting a coexistence region ($F_{3/2}+P$), $d=0.25$, $h=1.25$, and $T=0.25$. (f) Exhibiting a coexistence region ($F_{3/2}+F_{1/2}$), $d=-0.625$, $h=0.125$, and $T=0.05$. (g) Exhibiting a coexistence region ($F_{3/2}+F_{1/2}+P$), $d=-0.5$, $h=0.375$, and $T=0.0625$.

phase, and the second one is a second-order phase transition from the $F_{3/2}$ phase to the P phase and occurs. Therefore, the coexistence region, i.e., the $F_{3/2}+P$ phase, exists in the system and this fact is also seen in the phase diagram of Fig. 4(a) explicitly [compare in Figs. 2(f) and 2(g) with Fig. 4(a)]. Figures 2(h) and 2(i) show the thermal variations of M for $d=-0.75$, $h=0.35$ for two different initial values; i.e., the initial value of M is taken 3/2 or 1/2 for Fig. 2(h) and zero for Fig. 2(i). These figures are similar to Figs. 2(f) and 2(g), except the second-order phase transition is from the $F_{1/2}$ phase to the P phase and the first-order phase transition from the P phase to the $F_{1/2}$ phase. Therefore, the $F_{1/2}+P$ phase occurs in the systems [compare in Figs. 2(h) and 2(i) with Fig. 4(f)]. Finally, Figs. 2(j)–2(l) illustrate, which is the most interesting case, the thermal variations of M for $d=-0.475$, $h=0.375$ for three different initial values; i.e., the initial value of M is taken 3/2 for Fig. 2(j), and 1/2 for Fig. 2(k) and zero for Fig. 2(l). Figures 2(j)–2(l) are similar to Figs. 2(d), 2(e), and 2(g), respectively. However, in this case the system has the $F_{3/2}+F_{1/2}+P$ coexistence region [compare in Figs. 2(j)–2(l), with Fig. 4(c)].

Now we can check and verify the stability of the solution, and as well as the DPT points by calculating the Liapunov exponent λ. If we write Eq. (9) as follows:

$$\Omega\frac{dm}{d\xi} = F(m,\xi), \tag{12}$$

then the Liapunov exponent λ is given by

$$\Omega\lambda = \frac{1}{2\pi}\int_0^{2\pi}\frac{\partial F}{\partial m}d\xi. \tag{13}$$

When the Liapunov exponent is negative, the solution is stable. We have two Liapunov exponents in which one is

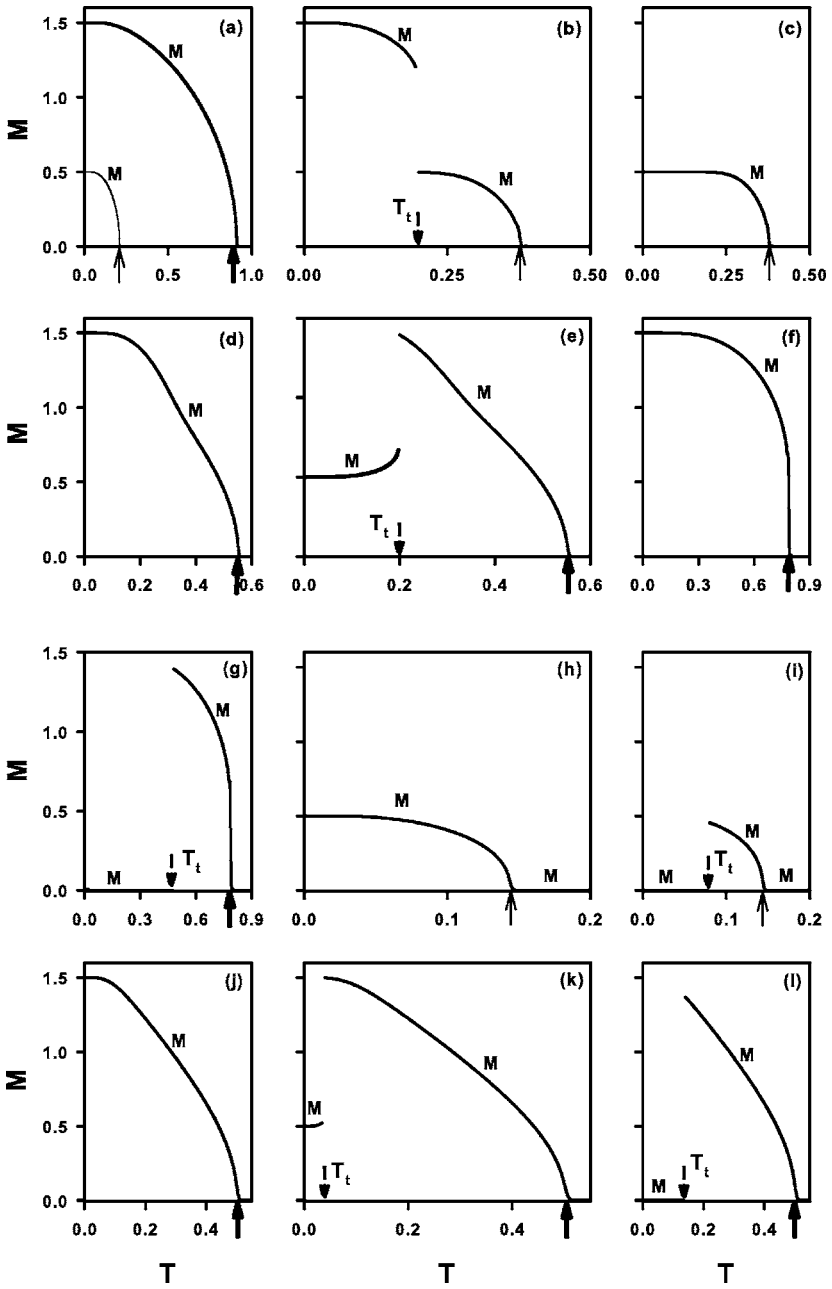

FIG. 2. The reduced temperature dependence of the dynamic magnetization M, and a symmetric solution which corresponds to the P phase, and nonsymmetric solutions that correspond to the $F_{3/2}$ and $F_{1/2}$ phases. T_t is the first-order phase transition temperatures, and T_C and $T_{C'}$ are the second-order phase transition temperatures from the $F_{3/2}$ phase to the P phase and the $F_{1/2}$ phase to the P phase, respectively. (a) Exhibiting two second-order phase transition, one from the $F_{3/2}$ phase to the P phase for $d=-0.25$, $h=0.50$; 0.915 is found T_C and the other one from the $F_{1/2}$ phase to the P phase for $d=-0.5$, $h=1.25$; 0.2125 is found $T_{C'}$. (b) Exhibiting two successive phase transitions, the first one is a first-order phase transition from the $F_{3/2}$ phase to the $F_{1/2}$ phase and the second one is second-order phase transition the $F_{1/2}$ phase to the P phase for $d=-0.50$ and $h=0.25$; 0.20 and 0.38 are found T_t and $T_{C'}$, respectively. (c) Exhibiting a second-order phase transition from the $F_{1/2}$ phase to the P phase for $d=-0.5$ and $h=0.25$; 0.38 is found $T_{C'}$. (d) Exhibiting a second-order phase transition from the $F_{3/2}$ phase to the P phase for $d=-0.475$ and $h=0.125$; 0.5575 is found T_C. (e) Exhibiting two successive phase transitions, the first one is a first-order phase transition from the $F_{1/2}$ phase to the $F_{3/2}$ phase and the second one is second-order phase transition the $F_{3/2}$ phase to the P phase for $d=-0.475$ and $h=0.125$; 0.20 and 0.5575 found T_t and T_C, respectively. (f) Same as Fig. 2(d), but $d=0.25$ and $h=1.025$; 0.795 is found T_C. (g) Exhibiting two successive phase transitions, the first one is a first-order phase transition from the P phase to the $F_{3/2}$ phase and the second one is second-order phase transition the $F_{3/2}$ phase to the P phase for $d=0.25$ and $h=1.025$; 0.48 and 0.795 found T_t and T_C, respectively. (h) Same as Fig. 2(c), but $d=-0.75$ and $h=0.35$; 0.1475 is found $T_{C'}$. (i) Same as Fig. 2(g), but the first-order phase transition from the P phase to the $F_{1/2}$ phase and the second-order phase transition is from the $F_{1/2}$ phase to the P phase, and $d=-0.75$ and $h=0.35$; 0.08 and 0.1475 found T_t and $T_{C'}$, respectively. (j) Same as Fig. 2(d), but $d=-0.475$ and $h=0.375$; 0.515 is found T_C. (k) Same as Fig. 2(e), but $d=-0.475$ and $h=0.375$; 0.04 and 0.515 are found T_t and T_C. (l) Same as Fig. 2(g), but $d=-0.475$ and $h=0.375$; 0.135 and 0.515 are found T_t and T_C.

associated to the symmetric solution, λ_S, and the other to the nonsymmetric solution, λ_n. If λ_s and λ_n increase to zero continuously as the reduced temperature approaches the phase transition temperature, the temperature where $\lambda_n=\lambda_s=0$ is the second-order phase transition temperature, T_C. On the other hand, if one of λ increases to zero continuously and the other λ jumps to zero discontinuously as the reduced temperature approaches to the phase transition temperature, the temperature in which the discontinuity occurs first for one of the λ and the other $\lambda=0$, is the first-order phase transition temperature, T_t. We should also mention that if the first-order phase transition is from the ordered phase to the disordered phase, λ_n increases to zero continuously and the other λ_S increases to zero discontinuously as the reduced temperature approaches the phase transition temperature. However, if the first-order phase transition is from one ordered phase to the other ordered phase, e.g., from the $F_{3/2}$ phase to the $F_{1/2}$ phase, one of the λ_n increases to zero continuously and the other λ_n increases to zero discontinuously as the reduced temperature approaches the phase transition temperature. In order to see these behaviors explicitly, the values of the Liapunov exponents are calculated and plotted as a function of the reduced temperature for $d=-0.5$ and $h=0.25$ [these values correspond to Fig. 2(b)], seen in Fig. 3(a) and for $d=-0.475$ and $h=0.375$ [these values correspond to Fig. 2(k)], as seen in Fig. 3(b). In this figures, the thick and thin lines represent the λ_s and λ_n, $\lambda_{n'}$, respectively, and T_t and T_C, $T_{C'}$ are the first- and second-order phase transition temperatures, respectively. In Fig. 3(a), the system undergoes two successive phase transitions: First, the phase transition is a first-order from the $F_{3/2}$ phase to the $F_{1/2}$ phase, because one of the $\lambda_n=0$ (λ_n corresponds to the $F_{3/2}$ phase) and the discontinuity occurs for the other $\lambda_{n'}$, which corresponds to the $F_{1/2}$ phase, and the first-order transition occurs at $T_t=0.20$; the second one is a second-order phase transition from the $F_{1/2}$ phase to the P phase, because $\lambda_n=\lambda_s=0$ at $T_{C'}=0.38$. The behavior of Fig. 3(b) is similar to Fig. 3(a), except the first-order phase transition is from the $F_{1/2}$ phase to the $F_{3/2}$ phase at $T_t=0.04$ and the second-order phase transition is from the $F_{3/2}$ phase to the P phase at $T_C=0.515$. If one compares Figs. 3(a) and 3(b) with Figs. 2(b) and 2(k), respectively, one can see that T_t and T_C, $T_{C'}$ found by using the both calculations, are exactly the same. Moreover, we have also verified the stability of the solutions by these calculations, because we have always found that $\lambda_s<0$, $\lambda_n<0$, and $\lambda_{n'}<0$.

We can now obtain the phase diagrams of the system and the calculated phase diagrams in the (T,h) plane are presented in Figs. 4(a)–4(f). In these phase diagrams the solid and dashed lines represent the second- and first-order phase transition lines, respectively, the dynamic tricritical points are denoted by a solid circle. As seen in Fig. 4, we have obtained six different phase diagrams topologies.

(i) For $d\geqslant -0.1982$, Fig. 4(a) represents the phase diagram in the (T,h) plane for $d=0.25$. In this phase diagram, at high reduced temperature (T) and the reduced external magnetic field amplitude (h) the solutions are paramagnetic (P) and at low values of T and h, they are ferromagnetic 3/2 $(F_{3/2})$. The dynamic phase boundary between these regions, $F_{3/2}\rightarrow P$, is the second-order phase line. At low reduced temperatures, there is a range of values of h in which the P and the $F_{3/2}$ phases or regions coexist, called the coexistence region, $F_{3/2}+P$. The $F_{3/2}+P$ region is separated from the $F_{3/2}$ and the P phases by the first-order phase line. The system also exhibits only one dynamic tricritical point where the both first-order phase transition lines merge and signals the change from first- to a second-order phase transitions. Finally, we should also mention that similar phase diagrams were also obtained in the kinetic spin-1 BC model [35], the kinetic of the mixed spin-1/2 and spin-1 Ising ferrimagnetic system [36] and as well as the kinetic spin-1/2 Ising model

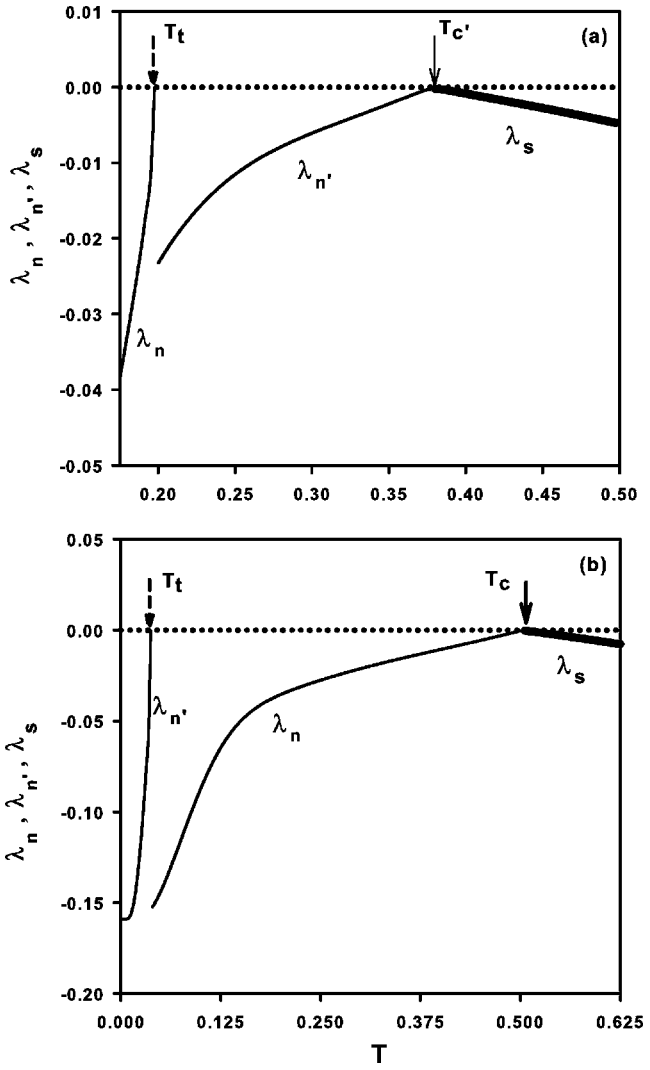

FIG. 3. The values of the Liapunov exponents as a function the reduced temperature. Thick and thin lines represent the λ_s, and λ_n, $\lambda_{n'}$, respectively, and T_t, and T_C, $T_{C'}$ are the first- and second-order phase transition temperatures, respectively. (a) The system undergoes two successive phase transitions: First, the phase transition is a first-order, because one of the $\lambda_n=0$ (λ_n corresponds to the $F_{3/2}$ phase) and the discontinuity occurs for the other $\lambda_{n'}$, which corresponds to the $F_{1/2}$ phase. The first-order phase transition occurs at $T_t=0.20$ and the second one is a second-order phase transition at $T_{C'}=0.38$, because $\lambda_n=\lambda_s=0$ for d=−0.5 and $h=0.25$. (b) Same as Fig. 3(a), but $d=-0.475$, $h=0.375$, and 0.04 and 0.515 are found T_t and T_C, respectively.

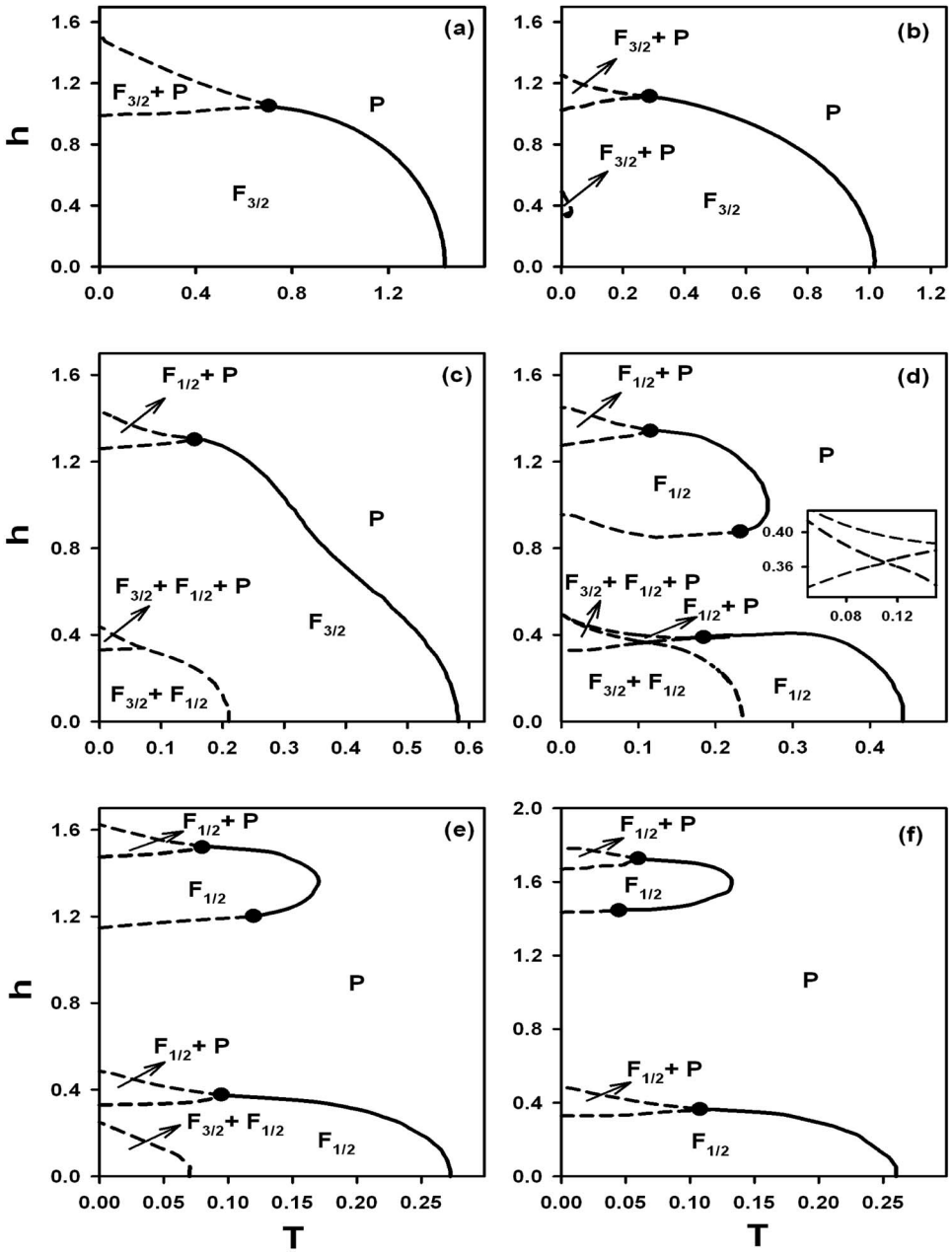

FIG. 4. Phase diagrams of the spin-3/2 Blume-Capel model in the (T,h) plane. The paramagnetic (P), ferromagnetic-3/2 $(F_{3/2})$, ferromagnetic-1/2 $(F_{1/2})$, and four different coexistence regions, namely the $F_{3/2}+P$, $F_{1/2}+P$, $F_{3/2}+F_{1/2}$, and $F_{3/2}+F_{1/2}+P$ regions, are found. Dashed and solid lines represent the first- and second-order phase transitions, respectively, and the dynamic tricritical points are indicated with solid circles. (a) $d=0.25$, (b) $d=-0.25$, (c) $d=-0.475$, (d) $d=-0.5$, (e) $d=-0.625$, and (f) $d=-0.75$.

[23]. The reason that the phase diagram is similar to the one obtained for the kinetic spin-1/2 Ising and spin-1 BC models are due to the competition between J, d, and h. If $d>0$, the Hamiltonian of spin-3/2 model gives similar results to the Hamiltonian of spin-1/2 Ising and spin-1 BC models. This can be seen explicitly from the ground state phase diagrams that we obtained in detail by Morita [42] and Canko and Keskin [43].

(ii) For $-0.1982>d\geqslant-0.2687$, we have performed the phase diagram at $d=-0.25$, seen in Fig. 4(b). This phase diagram is similar to Fig. 3(a) but only differs from Fig. 3(a) in which low T and h values one more of the $F_{3/2}+P$ phase or the coexistence region also exists. The dynamic phase boundary between this $F_{3/2}+P$ region and the $F_{3/2}$ phase is the first-order line, seen in Fig. 4(b).

(iii) For $-0.2687>d\geqslant-0.4887$, in this case the phase diagram is presented for $d=-0.475$, seen in Fig. 4(c). The system also exhibits one dynamic tricritical point that occurs in a similar place as in Fig. 4(a) and Fig. 4(b), but the coexistence region is the $F_{1/2}+P$ phase instead of the $F_{3/2}+P$. For low values of h and T, two more coexistence regions or phases exist, namely the $F_{3/2}+F_{1/2}+P$ phase occurs low values of T and high values of h and $F_{3/2}+F_{1/2}$ phase occurs very low values of T and h, seen in Fig. 4(c). The dynamic boundaries between these coexistence phases and between the coexistence regions and the $F_{3/2}$ phase are all first-order lines.

(iv) For $-0.4887>d\geqslant-0.5775$ the phase diagram is shown in Fig. 4(d) for $d=-0.5$. This is the more interesting phase diagram in which the system exhibits three dynamic tricritical points and also four coexistence regions or phases, namely two $F_{1/2}+P$ phases exist, one of them at very high values of h, at a similar place as in Fig. 4(c) and the other at low values of h; $F_{3/2}+F_{1/2}+P$ phase occurs at low values of

T and high values of h and the $F_{3/2}+F_{1/2}$ phase occurs at very low values of h and T, seen in Fig. 4(d). The dynamic boundaries between these coexistence phases are all first-order lines. The second-order phase line, that occurs at high values of h and separates the $F_{1/2}$ phase from the P phase, has a bulge that suggests the occurrence of the some sort of a reentrant phenomenon, because as the h value increases, the system passed from the ordered $(F_{1/2})$ phase to the disordered phase (P) and is then passed from the disordered (P) phase to the ordered $(F_{1/2})$ phase, and finally back to the P phase again. Moreover, at the end of this second-order phase line two dynamic tricritical points exist that one of them occurs in a similar place as in Fig. 4(c) and the other one at high values of T and low values of h. At zero T, there is a range of values of h in which P phase also exists and the dynamic phase boundaries between the P phase and ordered phases, namely the $F_{3/2}+F_{1/2}+P$ or $F_{1/2}$ phases, are the first-order phase lines. Furthermore, one more second-order phase line, which starts $h=0$ and ends a third dynamic tricritical point and separates the $F_{1/2}$ phase from the P phase, and exits in the system. The occurrence of the P phase at zero temperature has been also seen in the kinetic spin-1 BC model and the reason will be given in Sec. IV.

(v) For $-0.5775>d\geqslant-0.7350$, the phase diagram is obtained for $d=-0.625$, seen in Fig. 4(e), and is similar to case (iv), except that the $F_{3/2}+F_{1/2}+P$ region disappears and at zero T, there is a range of values of h in which the $F_{1/2}$ phase also exists. Therefore, the system exhibits three dynamic tricritical points and the $F_{1/2}+P$, $F_{3/2}+F_{1/2}$ coexistence regions besides the P and the $F_{1/2}$ phases.

(vi) For $-0.7350>d$, the phase diagram is similar to Fig. 4(e) but only differs from Fig. 4(e) in that very low T and h values of the $F_{3/2}+F_{1/2}$ region disappears, illustrated in Fig. 4(f). Hence, the system exhibits three dynamic tricritical points and the $F_{1/2}+P$ coexistence region besides the P and the $F_{1/2}$ phases.

IV. SUMMARY

We have analyzed within a mean-field approach the stationary states of the kinetic spin-3/2 Blume-Capel model under a time-dependent oscillating external magnetic field. We use Glauber-type stochastic dynamics to describe the time evolution of the system. We have studied the behavior of the time dependence of the magnetization and the behavior of the average magnetization in a period, also called the dynamic magnetization, as a function of reduced temperature. The DPT points are found by investigating the behavior of the average magnetization in a period as a function of the reduced temperature. These investigations are also checked and verified by calculating the Liapunov exponent. Finally, we present the phase diagrams in the (T,h) plane. We found that the behavior of the system strongly depends on the values of d and six different phase diagram topologies, where the P, $F_{3/2}$, $F_{1/2}$, $F_{3/2}+F_{1/2}$, $F_{3/2}+P$, $F_{1/2}+P$ or/and $F_{3/2}+F_{1/2}+P$ phases occur that depend on values of d, are found. The system also exhibits one or more tricritical points that depend on d values and the $F_{3/2}$, $F_{1/2}$ and/or $F_{3/2}+F_{1/2}$ phase occurs at low values of T and h. The reason that at low values of T, only the $F_{3/2}$ and the $F_{1/2}$ phases occur for the positive and negative high values of d, respectively, can also be seen from Eq. (9), analytically. While d goes to high positive and negative values, solutions of time-dependent magnetization should be $m(\xi)\sim\pm\frac{3}{2}e^{-\xi/\Omega}$ and $m(\xi)\sim\pm\frac{1}{2}e^{-\xi/\Omega}$, respectively. Hence, when $\xi\rightarrow\infty$, the stationary solutions of $m(\xi)$ always corresponds to the $F_{3/2}$ and the $F_{1/2}$ phases. Moreover, if one choice is a suitable value for h and negative values of d, one can obtain the P phase for low values of T, see in Figs. 4(e) and 4(f), explicitly. The P phase at suitable values of T and h appears in the phase diagrams as follows: For low values of T and h, due to the competition between T, h, and the decreasing d the time-dependent magnetization either follows the reduced magnetic field amplitude (h) within a single period, and $M=0$, this is the disordered or the P phase, or it cannot fully switch sign within a single period, and $|M|>0$, this is the ordered, namely the $F_{3/2}$ or the $F_{1/2}$ phases. On the other hand, for large and negative d, the paramagnetic phase becomes larger. Similar behavior has also been seen in the kinetic spin-1 BC model [35].

Finally, we should also mention that this mean-field dynamic study suggests that the spin-3/2 Blume-Capel model in the presence of a time-dependent oscillating external magnetic field has an interesting dynamic behavior, quite different from the standard Ising model. Therefore, it would be worthwhile to further study it with more accurate techniques such as dynamic Monte Carlo simulations or renormalization group calculations.

ACKNOWLEDGMENTS

This work was supported by the Technical Research Council of Turkey (TÜBİTAK) Grant No. 105T114 and Erciyes University Research Funds, Grant No. FBA-06–01.

[1] J. Sivardière and M. Blume, Phys. Rev. B **5**, 1126 (1972).
[2] S. Krinsky and D. Mukamel, Phys. Rev. B **11**, 399 (1975).
[3] See, e.g., N. Tsushima and T. Horiguchi, J. Phys. Soc. Jpn. **67**, 1574 (1998); O. Özsoy and M. Keskin, Physica A **319**, 404 (2003), and references therein.
[4] G. Refael, S. Kehrein, and D. S. Fisher, Phys. Rev. B **66**, 060402(R) (2002).
[5] A. Saguia, B. Boechat, and M. A. Continentino, Phys. Rev. B **68**, 020403(R) (2003).
[6] T. Kaneyoshi and M. Jaščur, Phys. Status Solidi B **173**, K37 (1992).
[7] G. Le Gal, T. Kaneyoshi, and A. Khater, Physica A **195**, 174 (1993).
[8] L. Peliti and M. Saber, Phys. Status Solidi B **195**, 537 (1996).

[9] J. A. Plascak, J. G. Moreira, and F. C. Sá Barreto, Phys. Lett. A **173**, 360 (1993).
[10] V. Ilkovič, Physica A **234**, 545 (1996).
[11] J. C. Xavier, F. C. Alcaraz, D. Penã Lara, and J. A. Plascak, Phys. Rev. B **57**, 11575 (1998).
[12] D. Peña Lara and J. A. Plascak, Int. J. Mod. Phys. B **12**, 2045 (1998).
[13] S. Grollau, Phys. Rev. E **65**, 056130 (2002).
[14] J. A. Plascak and D. P. Landau, Phys. Rev. E **67**, 015103(R) (2003).
[15] O. Özsoy, E. Albayrak, and M. Keskin, Physica A **304**, 443 (2002).
[16] A. Bakchich, S. Bekhechi, and A. Benyoussef, Physica A **210**, 415 (1994).
[17] S. Bekhechi and A. Benyoussef, Phys. Rev. B **56**, 13954 (1997).
[18] C. Ekiz, Phys. Lett. A **325**, 99 (2004); C. Ekiz, J. Magn. Magn. Mater. **284**, 409 (2004).
[19] M. Keskin, M. A. Pınar, A. Erdinç, and O. Canko, Phys. Lett. A **353**, 116 (2006).
[20] B. C. S. Grandi and W. Figueiredo, Phys. Rev. E **70**, 056109 (2004).
[21] O. Canko and M. Keskin, Physica A **363**, 315 (2006).
[22] M. Keskin and O. Canko, Phys. Lett. A **348**, 9 (2005).
[23] T. Tomé and M. J. de Oliveira, Phys. Rev. A **41**, 4251 (1990).
[24] J. F. F. Mendes and E. J. S. Lage, J. Stat. Phys. **64**, 653 (1991).
[25] R. J. Glauber, J. Math. Phys. **4**, 294 (1963).
[26] M. Acharyya, Phys. Rev. E **56**, 2407 (1997); A. Chatterjee and B. K. Chakrabarti, *ibid.* **67**, 046113 (2003).
[27] S. W. Sides, P. A. Rikvold, and M. A. Novotny, Phys. Rev. Lett. **81**, 834 (1998); Phys. Rev. E **59**, 2710 (1999); G. Korniss, C. J. White, P. A. Rikvold, and M. A. Novotny, *ibid.* **63**, 016120 (2001); G. Korniss, P. A. Rikvold, and M. A. Novotny, *ibid.* **66**, 056127 (2002).
[28] B. K. Chakrabarti and M. Acharyya, Rev. Mod. Phys. **71**, 847 (1999).
[29] M. F. Zimmer, Phys. Rev. E **47**, 3950 (1993); M. Acharyya and B. K. Chakrabarti, Phys. Rev. B **52**, 6550 (1995); M. Acharyya, Phys. Rev. E **58**, 179 (1998); H. Fujisaka, H. Tutu, and P. A. Rikvold, *ibid.* **63**, 036109 (2001).
[30] H. Tutu and N. Fujiwara, J. Phys. Soc. Jpn. **73**, 2680 (2004).
[31] M. Khorrami and A. Aghamohammadi, Phys. Rev. E **65**, 056129 (2002).
[32] H. Jang and M. J. Grimson, Phys. Rev. E **63**, 066119 (2001); H. Jang, M. J. Grimson, and C. K. Hall, Phys. Rev. B **67**, 094411 (2003); H. Jang, M. J. Grimson, and C. K. Hall, Phys. Rev. E **68**, 046115 (2003).
[33] T. Yasui, H. Tutu, M. Yamamoto, and H. Fujisaka, Phys. Rev. E **66**, 036123 (2002); **67**, 019901(E) (2003).
[34] E. Machado, G. M. Buendía, P. A. Rikvold, and R. M. Ziff, Phys. Rev. E **71**, 016120 (2005).
[35] M. Keskin, O. Canko, and Ü. Temizer, Phys. Rev. E **72**, 036125 (2005).
[36] G. M. Buendía and E. Machado, Phys. Rev. E **58**, 1260 (1998).
[37] H. J. Jensen, *Self-Organized Criticality: Emergent Complex Behavior in Physical and Biological Systems* (Cambridge University Press, Cambridge, England, 1998); J. Marro and R. Dickman, *Nonequilibrium Phase Transitions in Lattice Models* (Cambridge University Press, Cambridge, England, 1999).
[38] K. Christmann, *Introduction to Surface Physical Chemistry* (Steinkopff Verlag, Darmstadt, 1991); E. Machado, G. M. Buendía, and P. A. Rikvold, Phys. Rev. E **71**, 031603 (2005).
[39] Y.-L. He and G.-C. Wang, Phys. Rev. Lett. **70**, 2336 (1993); J.-S. Suen and J. L. Erskine, *ibid.* **78**, 3567 (1997).
[40] Q. Jiang, H. N. Yang, and G. C. Wang, Phys. Rev. B **52**, 14911 (1995); Q. Jiang, H. N. Yang, and G. C. Wang, J. Appl. Phys. **79**, 5122 (1996).
[41] W. Kleemann, T. Braun, J. Dec, and O. Petracic, Phase Transitions **78**, 811 (2005).
[42] T. Morita, Phys. Lett. A **133**, 369 (1988).
[43] O. Canko and M. Keskin, Phys. Lett. A **320**, 22 (2003).